Journal of Energy Storage 51 (2022) 104548

Contents lists available at ScienceDirect

Journal of Energy Storage

journal homepage: www.elsevier.com/locate/est

Research papers

Development of stable porous silica-coated $Ca(OH)_2/\gamma$-Al_2O_3 pellets for dehydration/hydration cycles with application in thermochemical heat storage

L. Briones [a,*], C.M. Valverde-Pizarro [a], I. Barras-García [a], C. Tajuelo [a,b], E.S. Sanz-Pérez [a], R. Sanz [a], J.M. Escola [a,*], J. González-Aguilar [b], M. Romero [b]

[a] Group of Chemical and Environmental Technology, Rey Juan Carlos University, C/ Tulipán s/n, 28933 Móstoles, Spain
[b] Unit of High Temperature Processes, IMDEA Energy Institute, Avda. Ramón de la Sagra 3, 28935 Móstoles, Spain

ARTICLE INFO

Keywords:
Thermochemical heat storage
Concentrated solar power
CaO
Hydration cycles
Silica shell

ABSTRACT

Thermochemical heat storage based on the $CaO + H_2O \leftrightarrow Ca(OH)_2$ system is extremely promising in CSP plants that can reach medium to high temperatures, such as those equipped with tower and heliostats. However, the attrition of pure CaO pellets is a major drawback that hampers an actual commercial development. This work proposes the dip-coating of mixed $Ca(OH)_2/\gamma$-Al_2O_3 spherical and cylindrical pellets with dense silica and Al-MCM-41 (mesoporous silica) gels. The original hardness of pure $Ca(OH)_2$ pellets (<2 N) can be increased up to 31 N using 40 wt% alumina as binder and applying a silica coating. Both gels formed a hard calcium silicate layer upon calcination that helped keeping the structural integrity of the samples after dehydration/hydration cycles. The samples were tested in 10 consecutive cycles at dehydration and hydration temperatures of 600 °C and 250–425 °C, respectively. Cylindrical pieces displayed higher hardness values and hydration yields compared to the spherical counterparts. Interestingly, porous silica-coated cylindrical pellets achieved a remarkable hydration yield of 85% and presented a hardness value of 8 N after cycling. This was due to its porous nature and the composition of the coating, formed by thin sheets and small grains, which allowed preserving the outer porous structure of the pellet.

1. Introduction

The production of increasing amounts of energy from renewable sources and the use of carbon-neutral technologies is nowadays a worldwide goal. In EU, an intensive research and development effort currently focuses on achieving the requirements of the 2030 Climate and Energy Framework (reducing greenhouse gas emissions at least 55% from 1990 levels, increasing the share of renewable energy to at least 32% and improving the energy efficiency to at least 32.5%) [1,2]. The improvement of energy storage systems, new biofuels for transportation and heating, and the use of biomass for electrical power production appear among the main research topics. Since the global trends point to a higher penetration of renewable energy sources, such as solar or wind, which are intermittent, the development of efficient energy storage systems appears to be mandatory to fully leverage the actual potential of renewable energy, avoiding unwanted losses of energy. In the particular case of thermal applications (as for example, concentration solar power), an appropriate thermal energy storage system allows to eliminate the gap between energy capture and use as well as increase the efficiency of the whole procedure [3,4].

Different physical-chemical properties of the storage material (sensible heat, latent heat and reaction enthalpy) may be harnessed to accomplish thermal energy storage. Thermochemical heat storage is based on a reversible chemical reaction, which absorbs heat in the endothermic decomposition reaction and releases it in the exothermic recombination one (Eq. (1)):

$$A + \text{heat} \leftrightarrow B + C \quad (1)$$

The process basically consists of three steps: 1) charge – thermal decomposition of A with the energy captured during sunlight hours; 2) storage – of the energy, in the form of internal energy, while both products, B and C, are kept apart; 3) discharge – recombination with heat release during the absence of solar energy – [5,6].

The main advantages of thermochemical heat storage are the

* Corresponding authors.
E-mail addresses: laura.briones.gil@urjc.es (L. Briones), josemaria.escola.saez@urjc.es (J.M. Escola).

https://doi.org/10.1016/j.est.2022.104548
Received 25 November 2021; Received in revised form 15 February 2022; Accepted 26 March 2022
Available online 4 April 2022

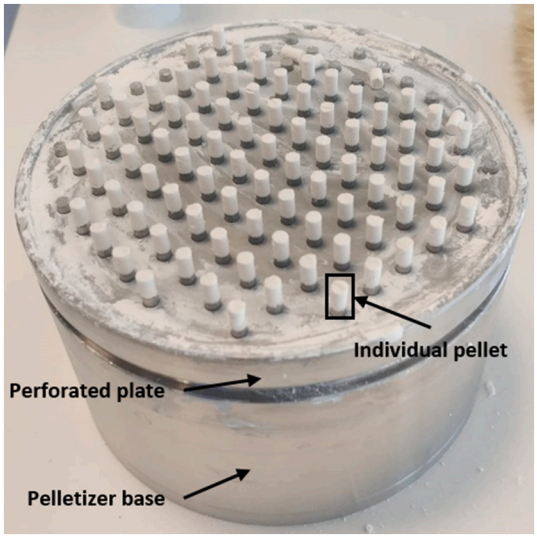

Fig. 1. Cylindrical pellets prepared in extruder.

opportunity for long-term storage as far as the products are kept separately, no thermal losses during storage at ambient temperature, and high energy density storage, 5 to 10 times larger than latent and sensible heat storage, respectively [7]. However, the storage system must display very important features, such as high reaction enthalpy, moderate reaction temperatures, good reversibility, fast reaction rates, stable products, large abundance, and low cost, among others [6–8]. In regard to the aforementioned characteristics, one of the most studied reactions has been the $CaO/Ca(OH)_2$ system. The dehydration/hydration cycle of calcium oxide is $Ca(OH)_2$ (s) ↔ CaO (s) + H_2O (g) + ΔH_R with ΔH_R = 104 kJ/ mol. This reaction presents a very high energy density (around 300 kWh m^{-3}), high reversibility (above 100 cycles), absence of by-products, easy separation of solid CaO and vapour, operation at atmospheric pressure and highly available and non-expensive reactants [7].

Many authors have investigated on this system, adjusting the reaction conditions and calculating kinetic and thermodynamic parameters [9–11], doping calcium with other elements [12–15], or evaluating different reactor set-ups [16–18]. There is a common agreement in literature to highlight two important drawbacks: pellets cracking and attrition, mainly due to the large volume change of the material, and crystallites agglomeration and sintering caused by continuous occurrence of high temperature, both phenomena leading to decline the material performance [19]. To offset these effects, several approaches have been proposed in recent years. A simple strategy was to mix CaO powders with large alumina particles in a fluidised bed reactor to minimize sintering [16]. Other approach was to use hydrophilic SiO_2 nanoparticles (Aerosil® A300) as fluidising agent. To procure a fine silica coating to the calcium hydroxide particles, both components were mixed in an intensive mechanical mixer and the hydration yield was measured after several dehydration/hydration cycles. Compared to the initial 100%, the hydration yield was reduced up to 94% along 10 cycles and the losses were attributed to pozzolanic reactions between $Ca(OH)_2$ and silica, conducing to the formation of calcium silicate, during the cycles [20,21].

A similar strategy is to prepare calcium based composite materials with improved mechanical properties. In this regard, many authors have doped CaO or $Ca(OH)_2$ with aluminium, nickel, copper, magnesium, zinc, or lithium [12,13,15]. In general, the effect of the dopant is to decrease the decomposition temperature of calcium hydroxide and to prevent nanoparticles to sinter [12,13]. However, Sakellariou and co-workers [22] reported that Ca/Al composite pellets made from calcium nitrate or acetate and aluminium nitrate precursors presented a combined crystalline phase, namely $Ca_3Al_2O_6$ and $Ca_{12}Al_{14}O_{33}$, which consumed part of the calcium and thus limited the hydration yield. This kind of pellets also fragmented during the second dehydration/hydration cycle, which points out that the mechanical properties were not improved. The authors concluded that a good material for this particular application should be a trade-off between hardness and hydration yield. Solid-solid reactions were also detected using a sodium silicate solution as binder in composite materials made of $CaCO_3$, $Ca(OH)_2$ and CaO, and calcined at 850 °C [20]. Two calcium silicates were identified by X-ray diffraction (XRD) analyses of the materials obtained, Na_2CaSiO_4 and Ca_2SiO_4, which are components of Portland cement. The presence of

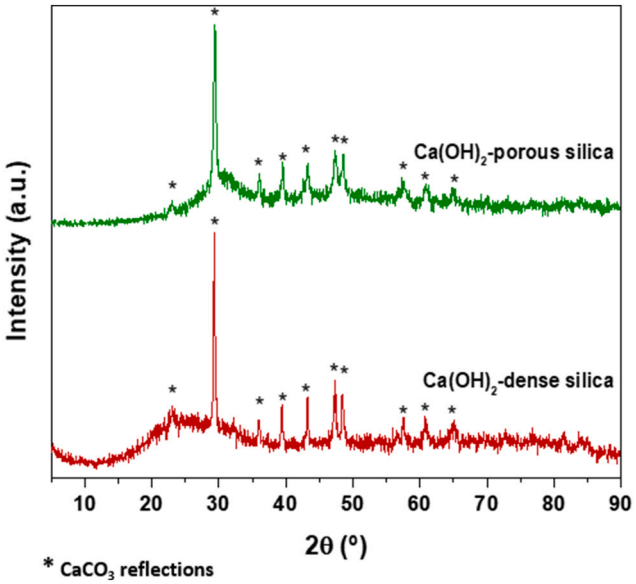

Fig. 3. X-ray diffractograms of the powders obtained from calcination at 500 °C of $Ca(OH)_2$ mixed with dense silica or mesoporous Al-MCM-41 gels.

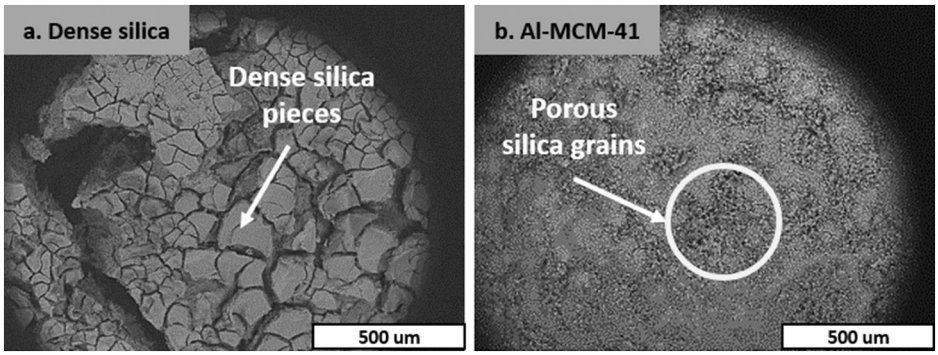

Fig. 2. Broadness of silica coverings over pure $Ca(OH)_2$ pellets. a) Dense silica. b) Mesoporous Al-MCM-41.

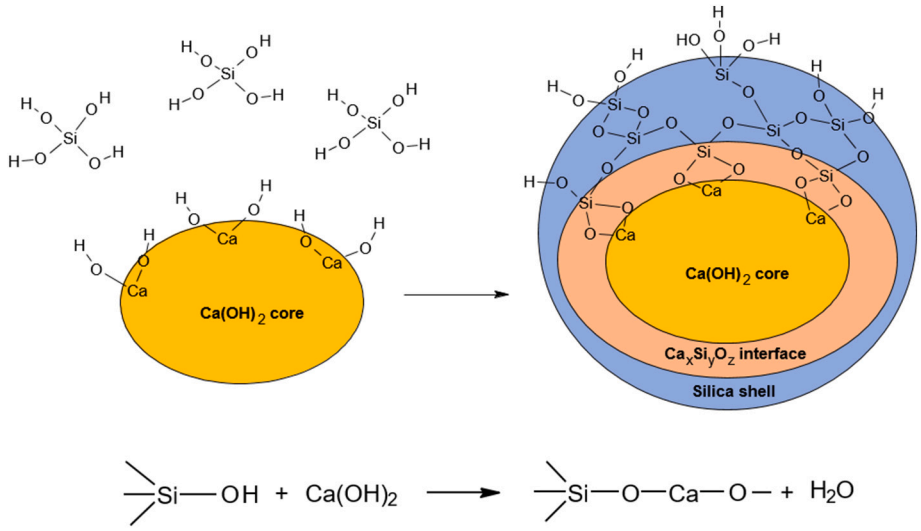

Fig. 4. Structure of the core-shell pellets and formation of a mixed Ca-O-Si intermediate layer.

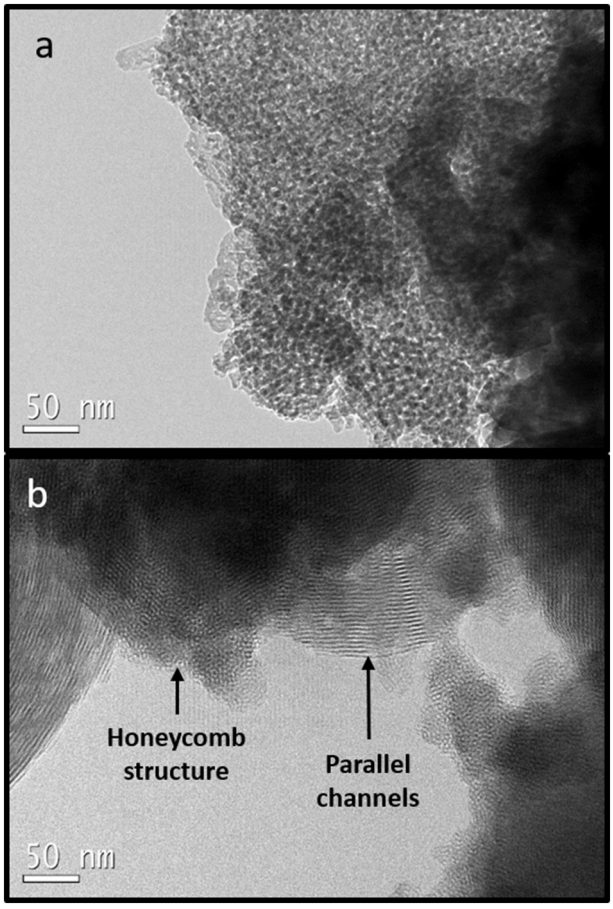

Fig. 5. TEM images of the porous silica coating. a) Coating scratched from a pellet. b) Powder recovered from the crucible after calcination of the pellets.

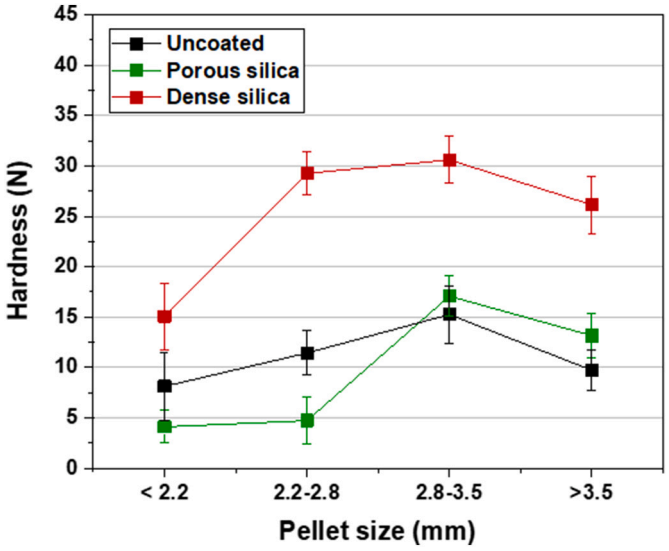

Fig. 6. Resistance to crushing of the coated and uncoated spherical mixed Ca $(OH)_2/\gamma$-Al_2O_3 pellets of different sizes.

these species provided higher mechanical resistance to the composite materials, above 17 N, but reduced the hydration yield of the samples compared to materials synthesized at lower temperatures in which the later silicate was not detected.

In other applications, such as CO_2 capture by CaO carbonation, similar problems were reported. The CO_2 capture declines very quickly for these materials along with the subsequent carbonation-calcination cycles, especially in the presence of steam, due to sintering of the CaO particles. Several solutions have been proposed in recent years. The coating of CaO nanoparticles with a ZrO_2 layer also led to a mixed interphase of $CaZrO_3$ or $CaZr_4O_9$ which prevented significant sintering up to 20 cycles [21]. A calcium titanate coating has also been used to prevent sintering of CaO nanoparticles [23]. Mesoporous zirconia has been employed to coat CaO pellets, showing both less sintering during the cyclic high temperature stages and good resistance to attrition. The mesoporous shell also facilitated CO_2 diffusion to and from the core for the 20 carbonation-calcination cycles tested [24]. Alumina, ceria and yttrium-stabilized zirconia were also used as shells, alumina being the most resistant material to attrition [25]. Core-shell materials have also been prepared from calcium carbonate (core) and clay powder (shell) by impregnating the cores with a clay slurry and drying repeatedly. Pellets larger than 4 mm size with a 0.45 mm thickness shell presented a resistance to crushing of 35 N and a mass loss by attrition of 0.035 wt %/h [26]. Calcium pellets doped with magnesium or aluminium species, calcium lignosulfonate or sepiolite also maintained high carbonation

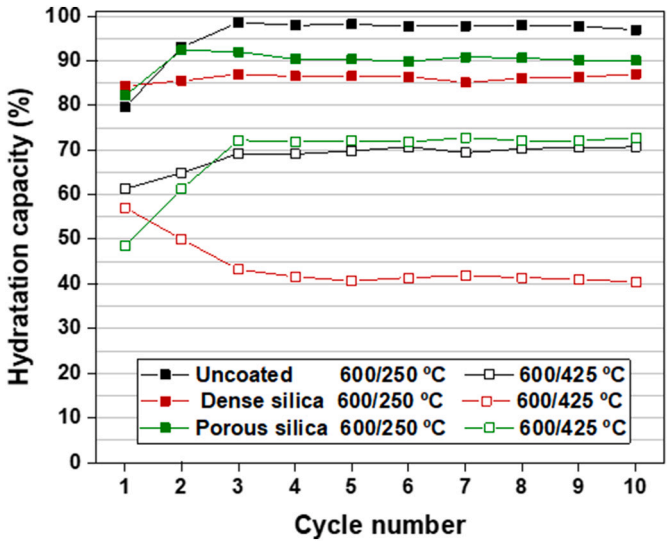

Fig. 7. Hydration capacities of the mixed $Ca(OH)_2$-Al_2O_3 spherical pellets in ten-cycle dehydration/hydration experiments at different temperatures. (For interpretation of the references to colour in this figure, the reader is referred to the web version of this article.)

yields for up to 50 cycles [27–32]. Another strategy has been the incorporation of calcium sorbents into porous supports to prevent sintering, such as MCM-41, SBA-15 or KIT-6. The main disadvantage of this approach is that the calcium load is limited by the total pore volume of the support [33–36].

In a previous work [37], the authors combined the core-shell strategy and the doping with aluminium and prepared 60 wt% $Ca(OH)_2$–40 wt% Al_2O_3 pellets coated with different mesoporous aluminas by dip-coating. The alumina coverings were obtained by a sol-gel method at several pH values and with or without an organic cationic surfactant. After 20 dehydration-hydration cycles, the sample A2 CS (neutral pH and surfactant) preserved its structural integrity and reached a constant hydration yield of ≈90% along the cycles. This work deals with the investigation on new coatings able to form a hard resistant shell and enhance the mechanical strength of the pellets while keeping high and stable hydration yields. The main goal is to provide valid materials that can be used in medium-high temperature CSP plants, such as those with tower reactors and nitrate salts as heat transfer fluid. In this regard, since pellets would not be able to fluidise, they would be placed into a fixed bed reactor, so thermal stress would be the main structural strain to cope with. Gels leading to dense silica and mesoporous Al-MCM-41-type silica (hereafter, porous silica) have been prepared and impregnated on the mixed cores (60% wt. $Ca(OH)_2$/40% wt. γ-Al_2O_3) by dip-coating. These pellets were manufactured with diverse shapes and sizes. The performance and ability to resist thermal stress of the shaped material under different hydration conditions were assessed for several cycles of dehydration/hydration and its relation with the synthesis procedure was established.

2. Experimental procedure

2.1. Preparation of the pellets

Dense silica gels were prepared by alkoxide hydrolysis and condensation routes published elsewhere [38–40] using tetraethyl orthosilicate (TEOS, Sigma-Aldrich, 98%) as precursor. The preparation of the gel begins with the dissolution of TEOS in ethanol and the hydrolysis of the alkoxide by adding 1 M HCl followed by stirring under reflux at 60 °C for 90 min and then at 40 °C for 90 min. Condensation occurs at room temperature during 48 h without stirring. The gel leading to the mesostructured silica-alumina Al-MCM-41 (Si/Al molar ratio of 30) was prepared from TEOS, aluminium chloride hexahydrate (Sigma-Aldrich, 99%), dimethylamine (DMA, Sigma-Aldrich, 40% aqueous solution) and cetyltrimethylammonium bromide (CTABr, Sigma-Aldrich, ≥98%), according to a procedure reported elsewhere [41]. Initially, aluminium chloride is dissolved in a water-dimethylamine mixture. Then, the CTABr surfactant is added and the mixture is stirred until a clear solution is obtained. Finally, TEOS is added dropwise and the solution is stirred at room temperature for 4 h until a white gel is formed. MCM-41 is a mesostructured silica with uniform hexagonal channels of tuneable width between 2 and 10 nm. Since pure silica is mostly hydrophobic, for many applications some silicon atoms are replaced by aluminium, which lends a moderate acidic and hydrophilic character to the final materials [42]. Hence, in this work, we prepared the aforementioned Al-MCM-41 gel. To the best of our knowledge, this is the first time that Al-MCM-41 gels have been utilized in a dip-coating procedure to form a porous silica shell on the surface of $Ca(OH)_2$ pellets.

Commercial $Ca(OH)_2$ powder (Acros Organics, 98%) was used to synthesize the core of the pellets. Acid γ-alumina (Merck, 90%) was used as binder to increase the mechanical strength of the samples. 60 wt% of $Ca(OH)_2$ and 40 wt% of the binder were crushed together in a mortar to ensure a fine mechanical mixing and then a small amount of water was poured to form a malleable paste. Part of this cement was conformed into spherical pieces of various sizes (2–4 mm) and the rest was conformed into uniform cylindrical pieces of 3 mm diameter and 4 mm length using the extruder shown in Fig. 1. The wet paste was pressed into the holes of a perforated plate and let dry for some minutes to facilitate the removal of the pellets. Then, the plate was fitted in the male part of the extruder, so the points could move the pellets through the holes. About 50 cylindrical pellets of 3 mm diameter and 4 mm length were produced for each batch. The cores were dried at 110 °C for 2 h in an oven to remove any excess water.

Pure $Ca(OH)_2$ or $Ca(OH)_2$/γ-Al_2O_3 cores, both spherical and cylindrical, were impregnated by the different gels following a dip-coating procedure. A number of pellets were placed into a steel grid which was immersed into the gels for 2 s and then removed slowly from the gel. The impregnated pellets were then transferred to a ceramic crucible, dried at 80 °C for 2 h and then calcined at 500 °C for 3 h in stagnant air to obtain a hard, solid coating. Some of the bare cores, not impregnated, were calcined under the same conditions to obtain uncoated reference samples.

2.2. Structural and thermal characterization of the samples

The morphology, continuity and local composition of the coatings were determined by scanning electron microscopy (SEM) using a Hitachi TM-1000 apparatus equipped with an energy-dispersive X-ray spectroscopy (EDX) detector. SEM images were acquired before and after dehydration/hydration tests. Transmission electron microscopy (TEM) of some coatings was also performed using a JEOL JEM 2100 apparatus under an accelerating voltage of 200 kV and LaB_6 filament.

The mechanical resistance of the pellets to crushing under compression, before and after dehydration/hydration tests, was measured in a Chatillon MT Ametek dynamometer. A collection of 15 pellets of each sample were crushed and their respective average strengths and standard deviations were calculated. The crystalline phases present in the samples were determined by XRD in a Philips X'Pert MPD diffractometer using Cu-Kα radiation with a step size of 0.1° and a counting time of 2 s.

The textural properties of the coated pellets were obtained from the nitrogen adsorption/desorption isotherms a 77 K acquired in a Micromeritics Tristar 3000 device. For each analysis, a number of pieces were outgassed for 30 min. at 90 °C and then for 480 min. at 200 °C. Then, the reactors were carefully transferred to the analysis unit in order to prevent any breakage of the pellets. Specific surface areas were calculated according to the Brunauer-Emmett-Teller method and the total pore volumes were considered at $p/p_0 = 0.98$.

Table 1
Energy stored (kJ/kg) in each evaluated material at different conditions.

Coating	Spherical shape		Cylindrical shape
	T_{HYD} = 250 °C	T_{HYD} = 425 °C	T_{HYD} = 425 °C
Uncoated	955.7	690.2	502.9
Dense silica	858.2	394.4	579.8
Porous silica	888.3	719.8	836.2

Dehydration/hydration tests were carried out in a TG 209 F3 Netzsch Tarsus thermo-microbalance coupled with a water vapour generator. Dehydration stages were performed at 600 °C in argon flow (20 mL/min) and hydration was performed at 250 or 425 °C under a 0.96 g/h steam mass flow in argon. The samples were subjected to 10 consecutive cycles. Hydration capacities were calculated according to Eq. (2) from the mass increase in the hydration stage and were referred to the mass increase achieved under the same analysis conditions by a CaO powder obtained from calcination at 500 °C of the commercial $Ca(OH)_2$ and corrected to the theoretical amount of CaO in the pellet:

$$\text{Hydration capacity}(\%) = \frac{\text{TG mass gain (sample)}}{\text{TG mass gain (CaO)}} \cdot \frac{\text{sample weight}}{\text{CaO weight in sample}} \cdot 100 \quad (2)$$

Finally, the energies potentially released for each sample were calculated according to Eq. (3), assuming 104 kJ/mol (1854.6 kJ/kg) as the enthalpy of the CaO hydration reaction:

$$\text{Energy release}(\text{kJ/kg}) = 1854.6\ \text{kJ}\Big/\text{kg} \cdot \frac{\text{CaO weight in sample}}{\text{sample weight}} \cdot \text{hydration capacity} \quad (3)$$

3. Results

3.1. Deposition of a stable silica coating over pure $Ca(OH)_2$ pellets and evaluation of the core-shell interaction

Initially, dense silica and Al-MCM-41 gels were impregnated on pure calcium hydroxide spherical pellets in order to determine if a continuous coating on the pellet surface could be obtained as well as to devise the kind of core-shell interaction that occur. As proved by SEM images in Fig. 2, both types of silica widely coated the surface of the pellets. Dense silica formed a thick and continuous layer all along the pellets surface. This shell was fractured into pieces upon drying and calcination at 500 °C, giving rise to cracks of different widths through which steam may diffuse. Al-MCM-41 gel did not formed a shell, but small grains distributed on the surface, similar to those observed by the authors on mesoporous alumina coatings [37].

The application of silica shells provides several important benefits. Firstly, the shell can act as a cement, avoiding material disaggregation during dehydration/hydration cycling. Moreover, fast solid-solid reactions between silica and calcium hydroxide have been reported in the literature leading to the formation of calcium silicates [20,24], which would improve the hardness of the pellets. Finally, the shell prevents the attrition of the core and the loss of part of this material in operating reactors.

The formation of the dense and porous silica flakes over the spherical $Ca(OH)_2$ pellets is due to a chemical interaction between the silica gel and the $Ca(OH)_2$ cores, as is proved by means of several experimental techniques. Fig. 3 shows the XRD patterns of the materials obtained from the calcination at 500 °C of $Ca(OH)_2$ powder impregnated with dense silica and Al-MCM-41 gels. All the observed crystalline reflections, marked with asterisks, correspond to $CaCO_3$ formed by carbonation of the hydroxide with atmospheric CO_2. It is noteworthy that calcium hydroxide impregnated with dense silica gel also gives rise to a broad shoulder centered at $2\theta \approx 23°$, which is typical of amorphous silica. However, this shoulder extends up to 35° and, in the case of the Al-MCM-41-impregnated sample (hereafter called porous silica), is clearly centered at $2\theta \approx 29.5°$, which indicates the presence of an amorphous calcium silicate or calcium-aluminium silicate hydrate [43–45]. No other crystalline phases, such as crystalline silicates, were detected. Although their presence cannot be completely ruled out, since species below 3 wt% or crystals smaller than 4 nm may not be detected by this technique, the formation of crystalline phases, such as β-$CaSiO_3$ or α-$CaSiO_3$, usually requires temperatures above 800 °C [46]. Hence, besides the silica sol-gel condensation and vitrification, a chemical bonding between $Ca(OH)_2$ and silanol groups is happening to form a Ca-O-Si species, as illustrated in Fig. 4.

This interaction between the calcium hydroxide and the silica gel also leads to a change in the porous structure and textural properties of the resulting shell when Al-MCM-41 gel is used. Fig. 5 shows TEM micrographs of the actual porous silica coating of a pellet (top image) and the powder formed during the calcination of some Al-MCM-41 gel deposited on the crucible but not attached to any pellet (bottom image), both obtained simultaneously after pellet calcination. The powder retrieved from the crucible presents the features of a mesostructured Al-MCM-41 silica-alumina, with the presence of parallel channels on the

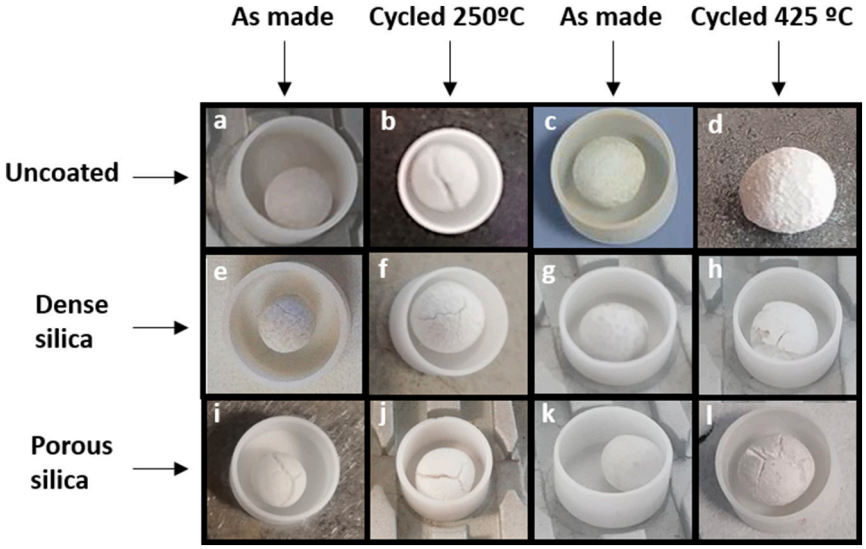

Fig. 8. Photographs of the spherical pellets before and after ten-cycle hydration experiments.

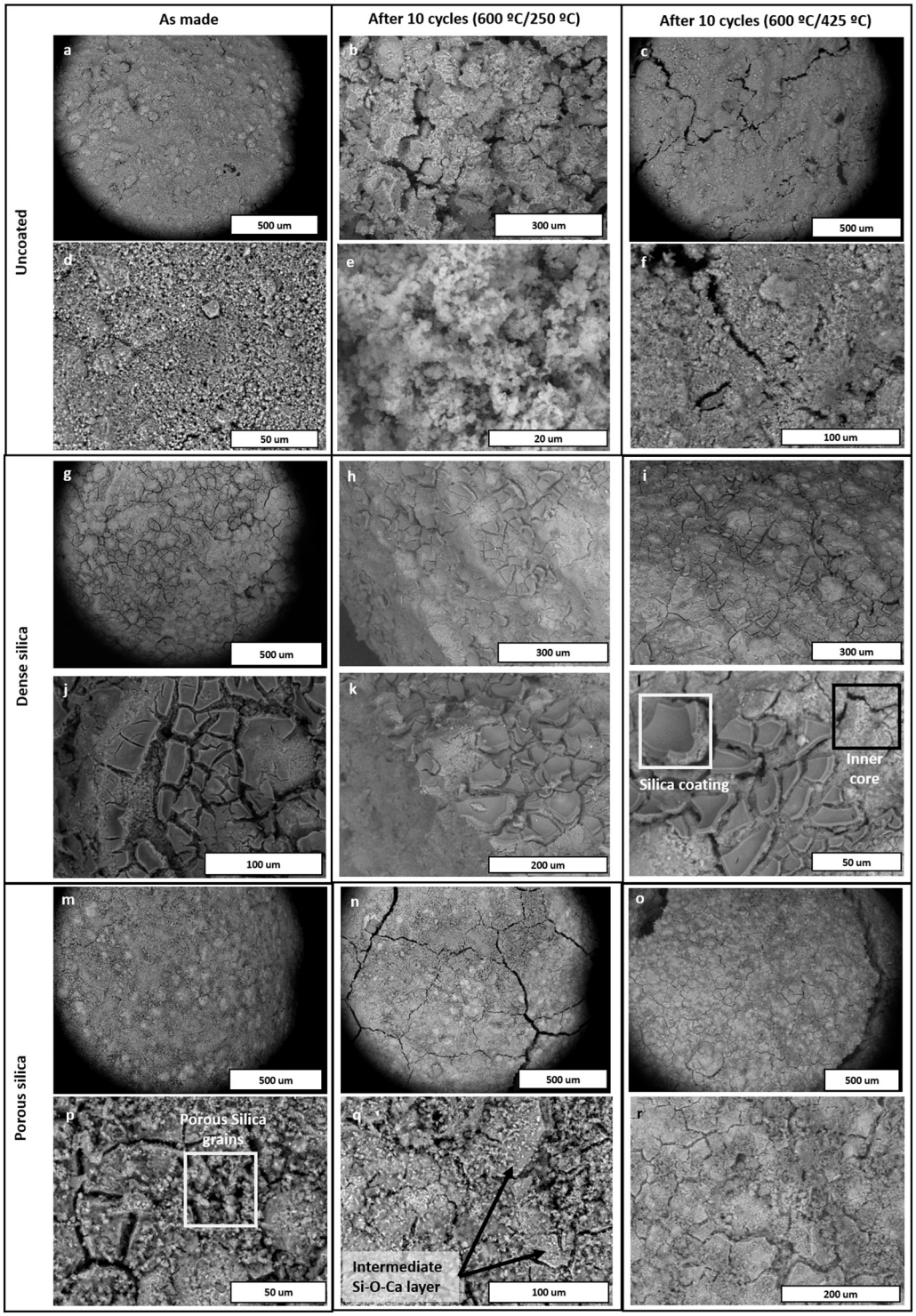

Fig. 9. SEM images of spherical pellets as synthesized and after 10 dehydration/hydration tests under different conditions.

longitudinal view and a hexagonal pattern on the transversal view. On the other hand, the material scratched from the pellet surface is made of small grains without any specific arrangement and is no longer a mesostructured Al-MCM-41. However, due to the presence and removal of the surfactant micelles during calcination, it is still porous, so it will be consider henceforth as a porous silica coating.

The observed differences between both silica coatings are caused by the different composition of the starting gels. First, dense silica gel is acidic because of the presence of HCl, while Al-MCM-41 gel is alkaline due to the presence of DMA. Moreover, Al-MCM-41 gel contains CTABr as a surfactant, which facilitates the interaction of the porous silica particles with the negatively charged surface of $Ca(OH)_2$ particles [47]. Finally, Al-MCM-41 gel contains aluminium (Si/Al molar ratio = 30) in its makeup, which, during calcination, may give rise to amorphous calcium aluminates or other Ca-Si-Al species [48]. The expected overall effect is a different kind of interaction between the gels and the surface of the calcium hydroxide particles forming the pellets.

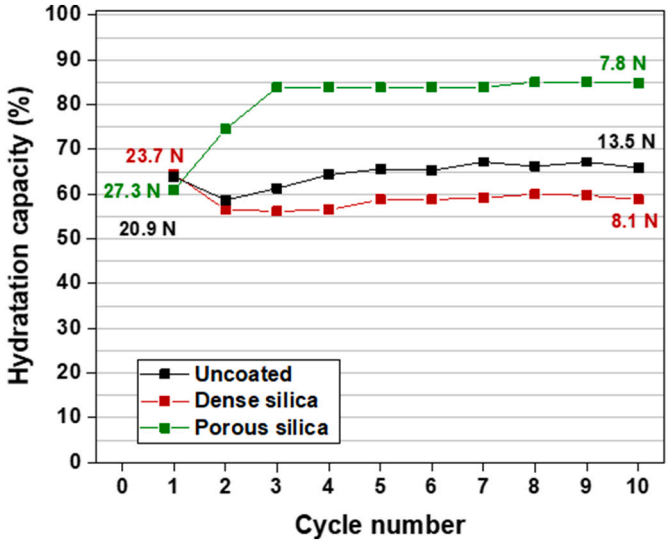

Fig. 10. Hydration capacities of the mixed $Ca(OH)_2/\gamma$-Al_2O_3 cylindrical pellets in ten-cycle experiments and hardness values before (left side) and after (right side) the experiments.

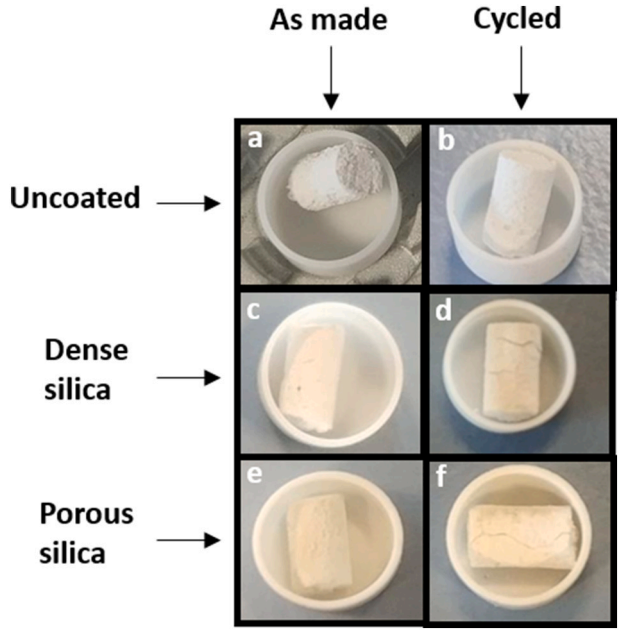

Fig. 11. Photographs of the cylindrical pellets before and after 10 dehydration/hydration cycles at 600 °C/425 °C.

3.2. Enhancement of the mechanical resistance of the pellets

One of the main drawbacks of pure calcium hydroxide pellets is their virtually negligible resistance to crushing (hardness < 2 N), so the addition of a hardening binder to the cores is necessary. In preliminary essays, several commercial and synthesized aluminas, as well as natural bentonite, were used as binders in proportions within the 10 wt%–50 wt % interval. It was observed that the highest hardness was achieved in a mixture 60 wt% calcium hydroxide and 40 wt% commercial alumina. Since the binder does not participate in the dehydration/hydration process, it is desirable to minimize its amount in the mixture. However, alumina has almost twice the density (≈4000 kg/m^3) of calcium hydroxide (≈2000 kg/m^3), so the volume occupied by a 40 wt% alumina in the final material is only 25%. Thus, pellets were made with the mixed paste, coated by the dip-coating procedure and calcined as described in Section 2.1. Additionally, some uncoated pieces were made following the same procedure and used as reference.

Spherical pieces were made and sorted into four groups according to their size: <2.2 mm, 2.2–2.8 mm, 2.8–3.5 mm and >3.5 mm. These sizes corresponded approximately to the following weights: <10 mg, 10–20 mg, 20–30 mg and >30 mg. Fig. 6 shows the mean and standard deviation of hardness values measured on mixed pellets, uncoated or coated with dense or porous silica and different sizes. Each point in the plot was obtained from, at least, 15 crushing measurements.

For the three types of material, the hardness of the pellets increases along with the size up to 3.5 mm. Above this diameter, lower strengths are measured. This phenomenon may be due to a lower width of the coating for the larger pellets, since the thickness of the shell decreases as the pellet radius increases. Thus, for example, according to gravimetric measurements carried out to a collection of pellets before and after coating, the mass percentage of dense silica for the 2.2–2.8 mm pellets is 16% on average, while it is only 1% for the >3.5 mm pieces. Therefore, pellets between 2.8 and 3.5 mm were utilized for further analyses.

Dense silica, which forms a continuous thick layer, leads to harder pellets than porous silica, which is made of small grains. The two intermediate sizes of the dense silica-coated pellets reached a hardness as high as 31 N. On the contrary, the highest value measured with porous silica is 17 N and it is quite similar to the hardness of the uncoated pieces. These values are comparable to those reported for similar materials [20,26,37].

It is noteworthy that, irrespectively of the coating material, the as-made samples, in spherical pellet form, presented quite high specific surface areas (≈58–61 m^2/g) and pore volumes (≈0.13–0.16 cm^3/g), showing as well the occurrence of both mesopores and macropores. This fact is particularly relevant considering that porosity favours steam diffusion inside and outside the pellets, finally resulting in higher hydration capacities. Thus, the preservation of the pellet porosity along the cycles is key for attaining high and stable hydration capacities.

In this regard, these materials were subjected to 10 consecutive dehydration/hydration cycles in order to check their hydration capacities. Dehydration stages were carried out at 600 °C and hydration stages at either 250 °C or 425 °C. 600 °C is the required temperature to achieve significant calcium carbonate decomposition [49]. Two dehydration temperatures were applied to evaluate the effect of this parameter in the hydration capacity of the samples as well as in their mechanical resistance. The obtained results are shown in Fig. 7, the solid colour symbols corresponding to the hydration tests at 250 °C and the empty ones to the tests at 425 °C.

Under 600 °C (dehydration)/250 °C (hydration) temperature conditions, the uncoated sample reached a sustained capacity of 97% of its theoretical maximum, so meaning that steam could actually reach the innermost part of the piece. In contrast, the presence of the coating reduced the hydration ability of the core-shell samples due to both diffusional limitation and the formation of calcium silicates. The calcium carbonate initially present in the samples is progressively decomposed during the first and second dehydration steps at 600 °C, so the hydration yield increases from the first cycle up to reaching a virtually constant value from the third cycle on, when decarbonation is complete. After 10 cycles, the porous silica-coated sample reached a hydration capacity of 90%, while the dense silica-coated material reached a slightly lower value, 87%. Despite the thick shell of the latter material, it shows only a slightly lower performance because steam can easily flow through the cracks and spaces between the silica sheets.

Under realistic operation conditions, hydration and dehydration temperatures must be as close as possible, thus a higher hydration temperature was also tested. By increasing the hydration temperature up to 425 °C the hydration capacities diminished for the three materials. The uncoated pellet and the porous silica-coated one reached 70% and 73% hydration yields from the third cycle on, respectively. Lower values compared to the previous conditions were expected because hydration is

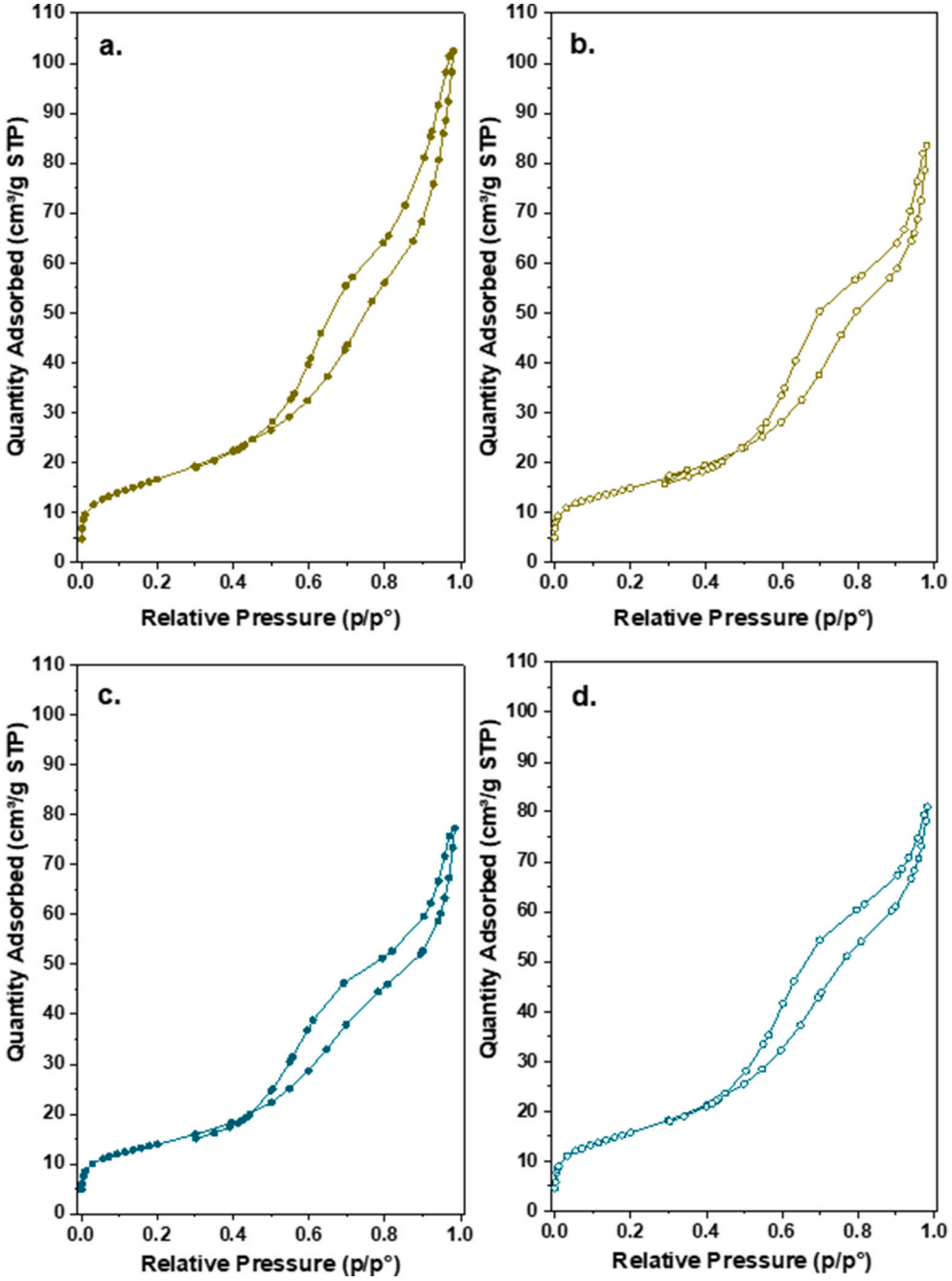

Fig. 12. N_2 adsorption/desorption isotherms before and after thermal stress tests. a) Dense silica-coated, spherical shape, before test. b) Dense silica-coated, spherical shape, after test. a) Porous silica-coated, cylindrical shape, before test. a) Porous silica-coated, cylindrical shape, after test.

thermodynamically hindered at higher temperatures [10] as well as by certain porosity loss by the CaO sintering at higher temperatures. Interestingly, the dense silica-coated material reached an initial yield similar to the other samples, around 57%, and then decreased to a constant value of 40%. This phenomenon suggests certain blockage of the inner porous structure of the pellet by displacement of the dense silica covering, additionally decreasing the porosity and hampering steam diffusion.

Table 1 gathers the stored energy in each material. The uncoated pellets would release 690 to 956 kJ per kilogram of material, depending on the conditions, the dense silica-coated ones 394 to 858 kJ/kg and the porous silica-coated ones 719 to 888 kJ/kg. It has to be taken into account that for the given proportion of CaO in all the materials, the maximum stored energy is 983 kJ/kg. It is clear that the porous silica-coated sample displays a much higher energy uptake, especially at the highest hydration temperature, which would be the closest to that of an actual operation, thus making this material a promising one for CSP plants.

The mechanical stability and durability of the pellets is also a very important aspect to consider. Due to thermal stress and large volume changes, pellets may break during the cycles. Besides, the decomposition of calcium carbonate, abruptly releasing back CO_2, may give rise to fragile structures, as previously described for CaO sorbents calcined at similar temperatures [50]. Although the fracture into large pieces does not reduce the hydration ability of the materials (on the contrary, it favours the steam and heat flows), the exposure of the soft cores can cause attrition, removal of fines and loss of material. Hence, it is undesirable on a long-term operation.

Table 2
Textural properties before and after 10 cycle experiments.

Property	Dense silica, spherical shape		Porous silica, cylindrical shape	
	Before	After	Before	After
BET surface area (m^2/g)	60	52	50	57
t-Plot external surface area (m^2/g)	58	44	42	52
Total pores volume at $p/p_0 = 0.98$ (cm^3/g)	0.157	0.128	0.115	0.122

To investigate on the effect of temperature and cycling on the silica shells, photographs and SEM micrographs before and after the ten-cycle experiments were acquired. Fig. 8 illustrates some photographs before and after the experiments. Cyclability assays causes superficial breakage due to volume changes and several large cracks are visible after the experiments in images f, j, h and l. Since the samples were calcined before the experiments and the final stage of the experiments was a hydration, the volume increase due to the conversion of CaO into $Ca(OH)_2$ is evident in the images, specially comparing photographs a to b, e to f and k to l. However, the pellets keep their spherical shape and integrity, which is in agreement with previously reported comparable materials [22,37].

Fig. 9 includes SEM micrographs of the surface of the samples as made and after 10 cycles at 600 °C/250 °C and 600 °C/425 °C. The uncoated material presents a smooth and even surface of CaO grains and the voids between the calcium oxide grains lend a certain porosity to the cores, which remains after the experiments, as can be seen in pictures d-f. In the case of the porous silica-coated material, the coating is made of two different layers, as can be appreciated in the detailed pictures p, q and r. The inner layer, which is immediately over the core, is made of small sheets containing calcium silicate. On top of that layer, grains of porous silica are visible. After cyclability experiments at 250 °C and 425 °C the two layers of coating are still visible and spreading all along the surface. As for the dense silica-coated materials, initially, thick silica sheets are located all along the surface but, underneath, the porous texture of CaO can be distinguished (images g and j). After the experiments, the silica tiles are still visible (images h, i, k and l). Therefore, both silica coatings seem to be strongly attached to the cores, although the extension and depth of the coating is bigger for the dense silica covering, which eventually would compromise the hydration capacity of the samples, as stated before.

3.3. Evaluation of the external morphology of the pellets

In addition to the spherical pellets, cylindrical pieces were made using an extruder. These samples were subjected to dehydration/hydration cycles at 600 °C/425 °C and hardness measurements before and after the cyclability test. Fig. 10 illustrates the hydration capacity as a function of the cycle for cylindrical pieces.

Fig. SI 1 in the Supporting information gathers the weight oscillations registered by the TG for all the materials tested in 10-cycle experiments at 600 °C/425 °C, both spherical and cylindrical. For all the samples, the first two dehydration stages comprise a fast dehydration process followed by a slower decarbonation. From the third cycle on, only dehydration occurs. This dehydration is almost immediate as the temperature starts rising from 425 °C to 600 °C and the atmosphere changes to pure Argon, and the lines corresponding to weight losses are almost vertical, irrespectively of the material. Therefore, no significant changes in the dehydration kinetics can be ascribed to the pellets composition. A close correspondence between mass losses and gains can be appreciated for all the cycles from the third one on. Thus, all the material that can be dehydrated in every sample can also be re-hydrated subsequently and this behaviour remains stable up to the final cycle. Since re-hydration kinetics are slower, any worsening in the performance of the pellets could be more evident in this stage. However, rehydration kinetics are rather similar from cycles 3 to 10.

The three cylindrical samples displayed high initial hardness values (21–27 N), within the same range of the spherical ones (15–31 N). It is noteworthy that, after the cycles, all three samples were recovered intact, as can be appreciated comparing the photographs of Fig. 11a to b, c to d and e to f, and their hardness values, although diminished, were still quite high, within the 8–14 N range. An abatement in the hardness of the pellets after the dehydration/hydration cycles was also observed by other authors [51].

During the hydration tests, the uncoated material showed a quite constant hydration capacity, around 65%. In the case of the pellet coated with porous silica, an increase in its hydration capacity up to the third cycle is detected and the final value is a remarkable 85%. On the contrary, the dense silica-coated pellets slightly decreased their hydration capacities from the first to the second cycle and then kept it constant at 60%, this abatement being lower than that of the spherical counterpart. Since the uncoated material also showed a small decrease in the hydration capacity in the second cycle, a possible explanation for this loss is the sintering of some CaO because of the high temperatures and a consequent reduction in the surface area and porosity. Although the doping of CaO with alumina has been proven to hamper the agglomeration of CaO particles [52,53], its occurrence was reported previously for alumina-coated $Ca(OH)_2/\gamma$-Al_2O_3 pellets [37] used in dehydration/hydration cycles. In that work, a growth from 14 nm to 59 nm (average) was calculated by the Scherrer equation after 5 subsequent cycles. CaO sintering is also favoured in the presence of CO_2 [54], so the release of carbon dioxide due to decarbonation in the first dehydration stages could enhance the effect.

However, although CaO sintering finally leading to porosity loss is likely occurring along the hydration/dehydration cycles, it does not equally affect all the samples, since the hydration capacity of the porous-silica coated pellet is hardly diminished. In the dense silica-coated material large amounts of silica are available for the formation of calcium silicate, which would rapidly fill most of the porosity of the outer surface and vitrify the pellet in the first stages. Instead, for the porous silica-coated pellet, the covering is not thick and continuous enough to form a large amount of calcium silicate, so the porosity loss due to its formation is limited. Additionally, the porous silica coating would hinder the aggregation of CaO moieties into bigger crystals over the external surface.

The change in the textural properties caused by high temperature was measured by the N_2 adsorption-desorption isotherms at 77 K. Since physisorption analyses require 5 to 10 pellets to be performed, we have subjected a number of pieces to a thermal treatment for 10 h at 600 °C to simulate the high temperature condition inside the TG apparatus. The samples with the best (porous silica-coated and cylindrical shape) and worst performance (dense silica-coated and spherical shape) in dehydration/hydration analyses were chosen to simplify the comparison and the isotherms were acquired before and after the thermal treatment. Fig. 12 shows the corresponding isotherms and the textural properties are collected in Table 2. The isotherms are of type IV, according to the IUPAC classification, which is typical of mesoporous materials. Additionally, all the samples adsorb large amounts of nitrogen at high relative pressures ($p/p_0 > 0.8$) because of the presence of large mesopores and macropores. This porosity mainly corresponds to the gaps between CaO and alumina particles in the cores. These voids lay within the 2–100 nm interval and no particular pore size stands out. Initially, the dense silica-coated sample presents a higher volume of pores, about 0.16 cm^3/g, compared to the porous silica-coated one, with 0.12 cm^3/g. This phenomenon may be ascribed to the nature of the coating. Since dense silica forms a thick and continuous layer, the outer surface of the pellets cannot accommodate to volume changes and gases release during calcination and breaks into diverse cracks, which is the origin of the additional amount of large pores and voids. With continuous high temperature, calcium silicate is formed and the more exposed CaO sinters. Thus, the thermally treated pellets present 20% less pores volume,

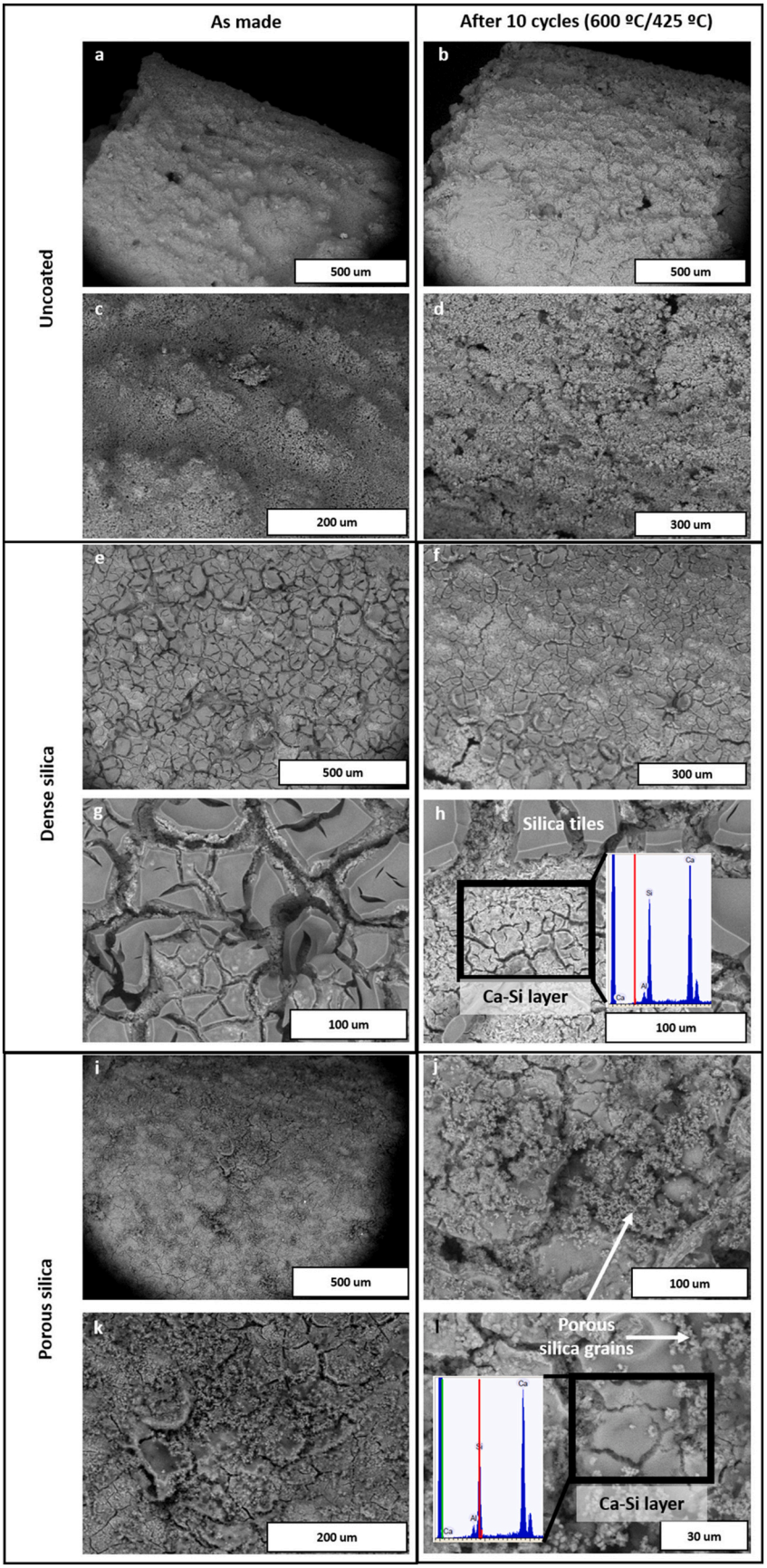

Fig. 13. SEM images of the cylindrical pellets as made and after 10 dehydration/hydration cycles at 600 °C/425 °C.

Table 3
Hydration yields (%) for the 10th cycle for all the tested pellets.

Pellets		Hydration yields (wt%)[a]	Hydration yields (wt%)[b]
Spherical $Ca(OH)_2$/ γ-Al_2O_3 (60/40 w/w)	Uncoated	97	70
	Dense silica coating	87	40
	Porous silica coating	90	73
Cylindrical $Ca(OH)_2$/ γ-Al_2O_3 (60/40 w/w)	Uncoated	–	65
	Dense silica coating	–	60
	Porous silica coating	–	85

[a] Dehydration at 600 °C; hydration at 250 °C.
[b] Dehydration at 600 °C; hydration at 425 °C.

15% less BET surface area and 25% less external surface area than the original ones. On the other hand, the porous silica coating is mainly granular and creates less tensional forces on the pellets surface, thus stabilizing the outer layers. Besides, this coating is thinner, so less calcium silicate forms. Temperature causes a slight cracking of the coating, augmenting the amount of large pores. The result is an increase of 15% in the BET surface area and 6% in the total pores volume.

The surface of the pieces before and after the experiments was further analysed from the SEM images in Fig. 13. The dense silica fragments still covered the pellet after the experiment but appeared to be thinner or more attached to the core, as can be seen in images e and f. Besides, in picture h, below the evident silica tiles, a new intermediate layer can be observed and EDX analyses prove that is made of both silicon and calcium in, approximately, 35% and 65%, respectively. This confirms the presence of a mixed Si—Ca phase that is visually distinguishable from the core material and the silica sheets. On the other hand, with the porous silica coating (image l), EDX analyses confirmed the occurrence of the intermediate tiles made up of silicon and calcium, although with a lower content of silicon in this case, about 25% Si and 75% Ca. In both materials, EDX also detected a small amount of aluminium, about 5–10%, coming from the alumina binder and/or the Al in the Al-MCM-41 gel.

Besides, the porous silica coating is originally hydrophilic because of the presence of aluminium, so the remaining unreacted silica must preserve its initially high ability to capture and diffuse water into the core. Thus, the good performance observed with the porous silica coating may be ascribed to both its porous nature and its ability to hold the porous structure of the pellet, avoiding pore blockage and enabling steam diffusion. These results are in agreement with those obtained for granular alumina coatings compared to lamellar ones, in which the hydration capacities were largely decreased compared to the former ones after 10 dehydration/hydration cycle experiments [37].

Comparing the performance of the spherical and cylindrical pellets in the dehydration/hydration test at 600 °C/425 °C, all the samples presented a very similar hydration yield for the first cycle, diverging from there. The reader can refer to Table 3 to find the final hydration yield of all the samples under the different analyses conditions. The uncoated pieces showed a very similar evolution, with final hydration yield around 65–70%. As for the coated samples, the cylindrical pieces reached about 10–15% higher sustained hydration capacities compared to their spherical counterparts. In this regard, as summarised in Table 1, the cylindrical pieces could store higher amounts of energy, from 503 to 836 kJ/kg. Additionally, the final hardness of the spherical pieces was quite low, below 5 N, while the cylindrical pieces kept moderate or high values.

The differences between the spherical and cylindrical pieces, regarding to hardness values, calcium silicate formation and hydration capacity, may be ascribed to two factors. A higher pressure applied to the pellets during their conformation with the extruder would make the cylinders harder. However, the shape itself is also important, for these particular cylinders have more surface compared to the spheres and thus the dynamometer requires more pressure to break them. Besides, a higher surface area of the pellets is in contact with the silica gels during the dip-coating procedure, so the overall coating/core ratio must be higher for the cylinders. A larger surface area also means a higher reaction surface for the calcium silicate to form and for the steam to access the material, decreasing diffusional hindrances, which would explain the higher hydration yields. Finally, is has to be taken into consideration that cylindrical pieces could accommodate better inside the reactor, reducing the void space and providing a higher energy uptake.

According to the obtained results, cylindrical alumina-mixed pellets coated with porous silica are a promising material for a larger scale application in thermochemical heat storage.

4. Conclusions

Pure and mixed CaO pellets were covered with silica materials following a dip-coating procedure and tested on dehydration/hydration cyclability tests at several temperatures. Dense silica gel gave rise to a true continuous shell that provided high strength values (up to 31 N) to the pellets. Al-MCM-41 gel formed a thinner coating made up of a calcium silicate or calcium aluminium silicate layer and porous silica grains.

Large amounts of calcium silicate were formed along 10 consecutive dehydration/hydration cycles at 600 °C/425 °C on the dense silica-coated pellets. This phenomenon, along with CaO sintering, decreased the hydration yield because of the occlusion of the outermost pores. On the contrary, porous silica, due to its thinner and porous structure, aided to preserve the outer porosity of the pellets, thus facilitating steam diffusion.

Cylindrical pellets presented higher surface areas to volume ratios than spherical counterparts did, which translates into an enhanced steam transport and increased mechanical stability. Hence, after the cyclability tests, cylindrical pieces kept a meaningful resistance to crushing (>8 N). Besides, cylindrical porous silica-coated pellets achieved a remarkable 85% hydration yield, equivalent to an energy uptake of 836 kJ/kg, which make them promising for an actual application in thermochemical heat storage.

Supplementary data to this article can be found online at https://doi.org/10.1016/j.est.2022.104548.

CRediT authorship contribution statement

L. Briones: Formal analysis, Investigation, Methodology, Visualization, Writing – review & editing. **C.M. Valverde-Pizarro:** Data curation, Investigation. **I. Barras-García:** Investigation. **C. Tajuelo:** Data curation, Investigation. **E.S. Sanz-Pérez:** Resources, Software. **R. Sanz:** Conceptualization, Project administration, Validation, Writing – review & editing. **J.M. Escola:** Conceptualization, Formal analysis, Supervision, Writing – original draft, Writing – review & editing. **J. González-Aguilar:** Funding acquisition, Writing – review & editing. **M. Romero:** Funding acquisition.

Declaration of competing interest

The authors declare that they have no known competing financial interests or personal relationships that could have appeared to influence the work reported in this paper.

Acknowledgements

The authors wish to thank *Comunidad de Madrid* and *European Structural Funds* for their financial support to ALCCONES project (S2013/MAE-2985) and ACES2030-CM project (S2018/EMT-4319). C. M. Valverde-Pizarro and I. Barras-García thank *Comunidad de Madrid* for the funding through the grants PEJD-2017-PRE/AMB-4390 and PEJ-

2019-AI/IND-15395, respectively.

The TEM images were acquired at the National Centre of Electronic Microscopy at the Complutense University of Madrid.

References

[1] European Council, European Council Conclusions. EUCO 169/14, 2014.
[2] European Commission, Communication from the European Commission. Stepping up Europe's 2030 Climate Ambition. Investing in a Climate-Neutral Future for the Benefit of Our People, 2020.
[3] A.J. Carrillo, J. Gonzalez-Aguilar, M. Romero, J.M. Coronado, Solar energy on demand: a review on high temperature thermochemical heat storage systems and materials, Chem. Rev. 119 (2019) 4777–4816, https://doi.org/10.1021/acs.chemrev.8b00315.
[4] T.M.I. Mahlia, T.J. Saktisahdan, A. Jannifar, M.H. Hasan, H.S.C. Matseelar, A review of available methods and development on energy storage; technology update, Renew. Sust. Energ. Rev. 33 (2014) 532–545, https://doi.org/10.1016/j.rser.2014.01.068.
[5] A.H. Abedin, M.A. Rosen, Closed and open thermochemical energy storage: energy- and exergy-based comparisons, Energy 41 (2012) 83–92, https://doi.org/10.1016/J.ENERGY.2011.06.034.
[6] T. Yan, R.Z. Wang, T.X. Li, L.W. Wang, I.T. Fred, A review of promising candidate reactions for chemical heat storage, Renew. Sust. Energ. Rev. 43 (2015) 13–31, https://doi.org/10.1016/J.RSER.2014.11.015.
[7] P. Pardo, A. Deydier, Z. Anxionnaz-Minvielle, S. Rougé, M. Cabassud, P. Cognet, A review on high temperature thermochemical heat energy storage, Renew. Sust. Energ. Rev. 32 (2014) 591–610, https://doi.org/10.1016/J.RSER.2013.12.014.
[8] W.E. Wentworth, E. Chen, Simple thermal decomposition reactions for storage of solar thermal energy, Sol. Energy 18 (1976) 205–214, https://doi.org/10.1016/0038-092X(76)90019-0.
[9] S. Lin, Y. Wang, Y. Suzuki, High-temperature CaO hydration/Ca(OH)2 decomposition over a multitude of cycles, Energy Fuels 23 (2009) 2855–2861, https://doi.org/10.1021/ef801088x.
[10] F. Schaube, L. Koch, A. Wörner, H. Müller-Steinhagen, A thermodynamic and kinetic study of the de- and rehydration of Ca(OH)2 at high H2O partial pressures for thermo-chemical heat storage, Thermochim. Acta 538 (2012) 9–20, https://doi.org/10.1016/j.tca.2012.03.003.
[11] Y.A. Criado, M. Alonso, J.C. Abanades, Kinetics of the CaO/Ca(OH)2 hydration/dehydration reaction for thermochemical energy storage applications, Ind. Eng. Chem. Res. 53 (2014) 12594–12601, https://doi.org/10.1021/ie404246p.
[12] M.S. Murthy, P. Raghavendrachar, S.V. Smram, Thermal decomposition of doped calcium hydroxide for chemical energy storage, Sol. Energy 36 (1986) 53–62, https://doi.org/10.1016/0038-092X(86)90060-5.
[13] I. Fujii, M. Ishino, S. Akiyama, M.S. Murthy, K.S. Rajanandam, Behavior of Ca(OH)2/CaO pellet under dehydration and hydration, Sol. Energy (1994), https://doi.org/10.1016/0038-092X(94)90036-1.
[14] J. Yan, C.Y. Zhao, Thermodynamic and kinetic study of the dehydration process of CaO/Ca(OH)2 thermochemical heat storage system with Li doping, Chem. Eng. Sci. 138 (2015) 86–92, https://doi.org/10.1016/j.ces.2015.07.053.
[15] J. Yan, C.Y. Zhao, First-principle study of CaO/Ca(OH)2 thermochemical energy storage system by Li or Mg cation doping, Chem. Eng. Sci. 117 (2014) 293–300, https://doi.org/10.1016/j.ces.2014.07.007.
[16] P. Pardo, Z. Anxionnaz-Minvielle, S. Rougé, P. Cognet, M. Cabassud, Ca(OH)2/CaO reversible reaction in a fluidized bed reactor for thermochemical heat storage, Sol. Energy 107 (2014) 605–616, https://doi.org/10.1016/j.solener.2014.06.010.
[17] M.N. Azpiazu, J.M. Morquillas, A. Vazquez, Heat recovery from a thermal energy storage based on the Ca(OH)2/CaO cycle, Appl. Therm. Eng. 23 (2003) 733–741, https://doi.org/10.1016/S1359-4311(03)00015-2.
[18] F. Schaube, J. Schütz, A. Wörner, H. Müller-Steinhagen, De- and rehydration of Ca(OH)2 in a reactor with direct heat transfer for thermo-chemical heat storage. Part B: validation of model, Chem. Eng. Res. Des. 91 (2013) 865–873, https://doi.org/10.1016/j.cherd.2013.02.019.
[19] K. Kudlacz, C. Rodríguez-Navarro, The mechanism of vapor phase hydration of calcium oxide: implications for CO2 capture, Environ. Sci. Technol. 48 (2014) 12411–12418, https://doi.org/10.1021/es5034662.
[20] Y. Álvarez Criado, M. Alonso, J.C. Abanades, Composite material for thermochemical energy storage using CaO/Ca(OH)2, Ind. Eng. Chem. Res. 54 (2015) 9314–9327, https://doi.org/10.1021/acs.iecr.5b02688.
[21] K.S. Sultana, D.T. Tran, J.C. Walmsley, M. Rønning, D. Chen, CaO nanoparticles coated by ZrO2 layers for enhanced CO2 capture stability, Ind. Eng. Chem. Res. 54 (2015) 8929–8939, https://doi.org/10.1021/acs.iecr.5b00423.
[22] K.G. Sakellariou, G. Karagiannakis, Y.A. Criado, A.G. Konstandopoulos, Calcium oxide based materials for thermochemical heat storage in concentrated solar power plants, Sol. Energy 122 (2015) 215–230, https://doi.org/10.1016/j.solener.2015.08.011.
[23] S.F. Wu, Y.Q. Zhu, Behavior of CaTiO3/nano-CaO as a CO2 reactive adsorbent, Ind. Eng. Chem. Res. 49 (2010) 2701–2706, https://doi.org/10.1021/ie900900r.
[24] Z. Sun, M.H. Sedghkerdar, J. Saayman, N. Mahinpey, N. Ellis, D. Zhao, S. Kaliaguine, A facile fabrication of mesoporous core–shell CaO-based pellets with enhanced reactive stability and resistance to attrition in cyclic CO2 capture, J. Mater. Chem. A 2 (2014) 16577–16588, https://doi.org/10.1039/C4TA03854A.
[25] M.H. Sedghkerdar, N. Mahinpey, A.H. Soleimanisalim, Z. Sun, Z. Chen, J. Lim, S. Kaliaguine, Core-shell structured CaO-based pellets protected by mesoporous ceramics shells for high-temperature CO2 capture, Can. J. Chem. Eng. 94 (2016) 2038–2044, https://doi.org/10.1002/cjce.22626.
[26] F.J. Liu, K.S. Chou, Y.K. Huang, A novel method to make regenerable core-shell calcium-based sorbents, J. Environ. Manag. 79 (2006) 51–56, https://doi.org/10.1016/J.JENVMAN.2005.05.013.
[27] H. Chen, C. Zhao, Development of a CaO-based sorbent with improved cyclic stability for CO2 capture in pressurized carbonation, Chem. Eng. J. 171 (2011) 197–205, https://doi.org/10.1016/J.CEJ.2011.03.091.
[28] H. Chen, C. Zhao, L. Duan, C. Liang, D. Liu, X. Chen, Enhancement of reactivity in surfactant-modified sorbent for CO2 capture in pressurized carbonation, Fuel Process. Technol. 92 (2011) 493–499, https://doi.org/10.1016/J.FUPROC.2010.11.002.
[29] H. Chen, C. Zhao, Y. Yang, P. Zhang, CO2 capture and attrition performance of CaO pellets with aluminate cement under pressurized carbonation, Appl. Energy 91 (2012) 334–340, https://doi.org/10.1016/j.apenergy.2011.09.032.
[30] F.N. Ridha, V. Manovic, A. Macchi, E.J. Anthony, High-temperature CO2 capture cycles for CaO-based pellets with kaolin-based binders, Int. J. Greenh. Gas Control. 6 (2012) 164–170, https://doi.org/10.1016/j.ijggc.2011.11.006.
[31] J. Shi, Y. Li, Q. Zhang, X. Ma, L. Duan, X. Zhou, CO2 capture performance of a novel synthetic CaO/sepiolite sorbent at calcium looping conditions, Appl. Energy 203 (2017) 412–421, https://doi.org/10.1016/j.apenergy.2017.06.050.
[32] B. Azimi, M. Tahmasebpoor, P.E. Sanchez-jimenez, A. Perejon, J. Manuel, Multicycle CO2 capture activity and fluidizability of Al-based synthesized CaO sorbents, Chem. Eng. J. 358 (2019) 679–690, https://doi.org/10.1016/j.cej.2018.10.061.
[33] F. Yu, N. Phalak, Z. Sun, L. Fan, Activation strategies for calcium-based sorbents for CO2 capture: a perspective, Ind. Eng. Chem. Res. (2012) 2133–2142, https://doi.org/10.1021/ie200802y.
[34] C.-H. Huang, K.-P. Chang, C.-T. Yu, P.-C. Chiang, C.-F. Wang, Development of high-temperature CO2 sorbents made of CaO-based mesoporous silica, Chem. Eng. J. 161 (2010) 129–135, https://doi.org/10.1016/J.CEJ.2010.04.045.
[35] H. Sun, C.M.A. Parlett, M.A. Isaacs, X. Liu, G. Adwek, Development of Ca/KIT-6 adsorbents for high temperature CO2 capture, Fuel 235 (2019) 1070–1076, https://doi.org/10.1016/j.fuel.2018.07.044.
[36] W. Liu, H. An, C. Qin, J. Yin, G. Wang, B. Feng, M. Xu, Performance enhancement of calcium oxide sorbents for cyclic CO2 capture—a review, Energy Fuel 26 (2012) 2751–2767, https://doi.org/10.1021/ef300220x.
[37] C.M. Valverde-Pizarro, L. Briones, E. Sanz, J.M. Escola, R. Sanz, J. González-Aguilar, M. Romero, Coating of Ca(OH)2/γ-Al2O3 pellets with mesoporous Al2O3 and its application in thermochemical heat storage for CSP plants, Renew. Energy 162 (2020) 587–595, https://doi.org/10.1016/j.renene.2020.08.095.
[38] N. Arconada, L. Arribas, B. Lucio, J. González-aguilar, M. Romero, Macroencapsulation of sodium chloride as phase change materials for thermal energy storage, Sol. Energy 167 (2018) 1–9, https://doi.org/10.1016/j.solener.2018.02.045.
[39] N. Arconada, A. Durán, S. Suárez, R. Portela, J.M. Coronado, B. Sánchez, Y. Castro, Synthesis and photocatalytic properties of dense and porous TiO2 -anatase thin films prepared by sol – gel, Appl. Catal. B Environ. 86 (2009) 1–7, https://doi.org/10.1016/j.apcatb.2008.07.021.
[40] N. Arconada, Y. Castro, A. Durán, Photocatalytic properties in aqueous solution of porous TiO2 -anatase films prepared by sol – gel process, Appl. Catal. A. Gen. 385 (2010) 101–107, https://doi.org/10.1016/j.apcata.2010.06.051.
[41] W. Lin, Q. Cai, W. Pang, Y. Yue, B. Zou, New mineralization agents for the synthesis of MCM-41, Microporous Mesoporous Mater. 33 (1999) 187–196, https://doi.org/10.1016/S1387-1811(99)00137-7.
[42] D.P. Serrano, G. Calleja, J.A. Botas, F.J. Gutierrez, Adsorption and hydrophobic properties of mesostructured MCM-41 and SBA-15 materials for volatile organic compound removal, Ind. Eng. Chem. Res. 43 (2004) 7010–7018, https://doi.org/10.1021/ie040108d.
[43] J.R. Houston, R.S. Maxwell, S.A. Carroll, Transformation of meta-stable calcium silicate hydrates to tobermorite: reaction kinetics and molecular structure from XRD and NMR spectroscopy, Geochem. Trans. 10 (2009) 1–14, https://doi.org/10.1186/1467-4866-10-1.
[44] G.M.N. Baston, A.P. Clacher, T.G. Heath, F.M.I. Hunter, V. Smith, S.W. Swanton, Calcium silicate hydrate (C-S-H) gel dissolution and pH buffering in a cementitious near field, Mineral. Mag. 76 (2012) 3045–3053, https://doi.org/10.1180/minmag.2012.076.8.20.
[45] Y. He, L. Lu, L.J. Struble, J.L. Rapp, P. Mondal, S. Hu, Effect of calcium-silicon ratio on microstructure and nanostructure of calcium silicate hydrate synthesized by reaction of fumed silica and calcium oxide at room temperature, Mater. Struct. Constr. 47 (2014) 311–322, https://doi.org/10.1617/s11527-013-0062-0.
[46] W. Xia, J. Chang, Preparation and the phase transformation behavior of amorphous mesoporous calcium silicate, Microporous Mesoporous Mater. 108 (2008) 345–351, https://doi.org/10.1016/j.micromeso.2007.04.013.
[47] J.T. Muth, J.A. Lewis, Microstructure and elastic properties of colloidal gel foams, Langmuir 33 (2017) 6869–6877, https://doi.org/10.1021/acs.langmuir.7b01476.
[48] R.E. Przekop, P. Marciniak, B. Sztorch, A. Czapik, A. Marty, New method for the synthesis of Al2O3 – CaO and Al2O3 – CaO – CaCO3 systems from a metallic precursor by the sol – gel route, J. Aust. Ceram. Soc. 54 (2018) 679–690, https://doi.org/10.1007/s41779-018-0197-0.
[49] I. Galan, F.P. Glasser, C. Andrade, Calcium carbonate decomposition, J. Therm. Anal. Calorim. 111 (2013) 1197–1202, https://doi.org/10.1007/s10973-012-2290-x.
[50] H. Sun, J. Wang, X. Liu, B. Shen, C.M.A. Parlett, G.O. Adwek, E. John Anthony, P. T. Williams, C. Wu, Fundamental studies of carbon capture using CaO-based

materials, J. Mater. Chem. A 7 (2019) 9977–9987, https://doi.org/10.1039/c8ta10472g.
[51] M. Gollsch, S. Afflerbach, M. Drexler, M. Linder, Structural integrity of calcium hydroxide granule bulks for thermochemical energy storage, Sol. Energy 208 (2020) 873–883, https://doi.org/10.1016/j.solener.2020.08.017.
[52] M. Benitez-Guerrero, J.M. Valverde, P.E. Sanchez-Jimenez, A. Perejon, L.A. Perez-Maqueda, Calcium-looping performance of mechanically modified Al2O3-CaO composites for energy storage and CO2 capture, Chem. Eng. J. 334 (2018) 2343–2355, https://doi.org/10.1016/j.cej.2017.11.183.
[53] H. Sun, Y. Li, X. Yan, J. Zhao, Z. Wang, Thermochemical energy storage performance of Al2O3/CeO2 co-doped CaO-based material under high carbonation pressure, Appl. Energy 263 (2020), 114650, https://doi.org/10.1016/j.apenergy.2020.114650.
[54] X.K. Tian, S.C. Lin, J. Yan, C.Y. Zhao, Sintering mechanism of calcium oxide/calcium carbonate during thermochemical heat storage process, Chem. Eng. J. 428 (2022), 131229, https://doi.org/10.1016/j.cej.2021.131229.